Journal of Thermal Analysis and Calorimetry
https://doi.org/10.1007/s10973-024-13580-z

Numerical investigation of a heat pipe receiver for the solar dish collector humidification–dehumidification desalination system

Mohammad Afarideh[1] · Pouya Esfanjani[1] · Mohammad Sadegh Valipour[1]

Received: 11 April 2024 / Accepted: 15 August 2024

Abstract

Regarding the increasing demand for freshwater supply worldwide in coming years, solar desalination systems have good potential for tackling this challenge. Solar humidification–dehumidification desalination system is a technology that can effectively supply the water demand for rural areas with brackish water resources. Parabolic dish collectors with cavity receivers are one of the heat source options for this desalination technique. The main challenge for a dish collector with a cavity receiver-based desalination system is the low freshwater production rate. The current research aims to utilize a heat pipe receiver in a dish collector to heat brackish water to the required temperature for the humidification–dehumidification desalination process. According to the results, the flow rate of the inlet brackish water varied between 0.3 and 0.4875 L min^{-1}, while the temperature of the outlet brackish water of the heat pipes ranged from 60.20 to 64.24 °C. Moreover, the results show that with the application of a heat pipe receiver, a maximum thermal efficiency of 35.79% was determined in the parabolic dish collector system for water sample with 10,600 µS cm^{-1} salinity. Moreover, 35.50, 35.30, and 35.08% were calculated for the average thermal efficiency values of the parabolic dish collector system for water samples with 3880, 10,600, and 21,500 µS cm^{-1} salinity, respectively. Also, the maximum outlet temperature for the brackish water samples with 3880, 10,600, and 21,500 µS cm^{-1} salinity were 63.98, 61.51, and 64.37 °C, respectively. According to the findings, heat pipe receivers lead to higher freshwater production rates than conventional cavity receivers.

Keywords Solar thermal desalination · Humidification–dehumidification desalination · Solar dish collector · Heat pipe receiver · Thermal performance

Abbreviations

$\dot{m}$	Brackish water mass flow rate, kg s^{-1}
T_{in}	Brackish water inlet temperature, °C
T_{out}	Brackish water outlet temperature, °C
T_s	Inner pipe surface wall temperature, °C
G	Solar irradiation, W m^{-2}
A_{dish}	Reflector aperture area, m^2
V	Working fluid velocity in vapor cavity, m s^{-1}
U	Working fluid velocity in wick, m s^{-1}
t	Time, s
K	Permeability of the porous wick, m^2
Q_m	Mass source, kg
L	Tube length, m
p	Tube perimeter, m
c_p	Heat capacity at constant pressure, J kg^{-1} K^{-1}

Greek symbols

β	Fluid phase
∇	Gradient
η_{th}	Thermal efficiency, %
ϵ_p	Wick porosity
μ	Dynamic viscosity of working fluid, Pa s
ρ	Working fluid density, kg m^{-3}

Subscripts

th	Thermal
o	Outlet
s	Surface
m	Mass
p	Pressure

Introduction

Water scarcity can be considered a serious global issue in the current world. The rising population trend and the countries' technological and economic developments have resulted in

✉ Mohammad Sadegh Valipour
msvalipour@semnan.ac.ir

[1] Faculty of Mechanical Engineering, Semnan University, Semnan, Iran

Published online: 16 September 2024

more water demand than before. Furthermore, freshwater global demand is expected to be two times greater than now by 2050 [1–3]. Desalination processes are among the best methods to tackle the challenges of water demands. The usual methods are based on thermal, electrical, or chemical processes for distilled water extraction from sea or brackish water [4–6]. Humidification–dehumidification (HDH) desalination cycles are the enhanced desalination method of solar stills. Besides solar stills, HDH systems are divided into two columns: humidifier and dehumidifier. There are two kinds of fluid-heating systems in the HDH method: water-heated and air-heated [7, 8]. Solar thermal collectors can be used in various energy systems applications, such as desalination [9–11]. They are used as a heat source, and based on the required temperature of the desalination technique, the suitable collector will be selected [12, 13]. Solar thermal collectors are categorized into two main categories: concentrating and non-concentrating [14, 11]. Solar collectors such as linear Fresnel reflectors, parabolic dish collectors, and parabolic trough collectors can be effectively used as heat sources of the desalination systems according to their working temperature range [14–19]. Parabolic dish collectors are suitable options for HDH systems due to their high solar concentration capability and efficient thermal performance [20, 21]. The solar HDH desalination cycle mechanism is based on the heating of saline water in a solar thermal collector. The heated water is transferred and sprayed in the humidifier column to humidify and warm the airflow. Then, the humidified air condenses its moisture into freshwater in the dehumidifier [22]. Rafiei et al. [23, 24], in two studies, theoretically investigated the integration of a parabolic dish collector (PDC) with the HDH desalination system. They used photovoltaic thermal panels to supply the electrical demand and preheat the water. Their investigated cavity receiver geometries were rectangular, cylindrical, and hemispherical. According to their results, the highest water productivity of 19 kg h^{-1} was reported by using the hemispherical cavity receiver. Esfanjani et al. [25, 26], studied a PDC-based HDH desalination system with a novel design of a cavity receiver with cylindrical–conical geometry. They conducted their experiments with brackish water resources of Semnan province to study the effect of salinity on freshwater productivity. Based on their results, 45.49% was reported for the highest thermal efficiency of the system. Moreover, they mentioned the highest water productivity of 0.966 L day^{-1}. The application of heat pipes in desalination systems is a novel idea that researchers have recently introduced and investigated. Hemmatian et al. [27] worked experimentally on a solar still integrated with an evacuated solar collector and heat pipe mechanism. They used the heat pipe cycle to heat the brackish water in the basin of the solar still to increase its performance. They reported 19.4% energy efficiency for their proposed system.

Heat pipes are an efficient heat transfer system that conducts heat from one side to another without using moving parts. As illustrated in Fig. 1, the heat pipe comprises the evaporator zone, condenser zone, adiabatic zone, working fluid and the wick [28, 29]. In a heat pipe, a wick of a specified thickness is positioned along the inner wall of a vacuum-sealed tube. The tube is charged with a working fluid. Following heat absorption from the evaporator region, the working fluid vaporizes, transitioning into vapor and directing to the condenser zone. In the condenser zone, working fluid releases its latent heat to the surroundings, undergoing condensation and changing into liquid phase. Due to capillary forces, the result is a pressure gradient in the liquid, which causes the liquid to flow through the wick toward the end of the evaporator in the opposite direction to the vapor flow in the vapor cavity and completes the flow cycle. This flow continues until the pressure difference in the pipe continues to exist [30]. Heat pipe is categorized in different shapes, such as cylindrical flat plate and closed loop [31, 32].

Heat pipes also operate in a wide temperature range. Water and phase change materials are used in low-temperature ranges, and in high temperatures, sodium, and potassium are used as working fluids [32–35]. Several studies have been conducted on the thermal efficiency of heat pipes in the past decade. Faghri and Buchko [36], studied numerically and experimentally the impact of thermal flux distribution on steam temperature and pipe wall in a cylindrical heat pipe. Their investigated copper heat pipe was 1m long, and the outer and inner diameters were 25.4 and 2 mm, respectively. A porous copper metal thickness of 0.712 mm was used as a wick, and water was used as a working fluid at 60–100 °C temperature. The evaporator area of 4 heat sources that together had a maximum power of 257 W, and the length of each was 63.5 mm. The condenser's length was 300 mm, and the adiabatic area was insulated by a ceramic fiber with a thickness of 50 mm. Their tests were performed in different conditions involving heat source powers. The heat pipe's wall temperature with a single heat source set at 100 W was 75 °C, while for 4 heat sources of 50 W, this value

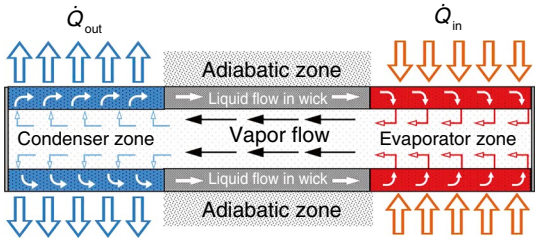

Fig. 1 The overall function of the heat pipe, which consists of the evaporator area, the condenser area, the adiabatic area, the working fluid, and the wick

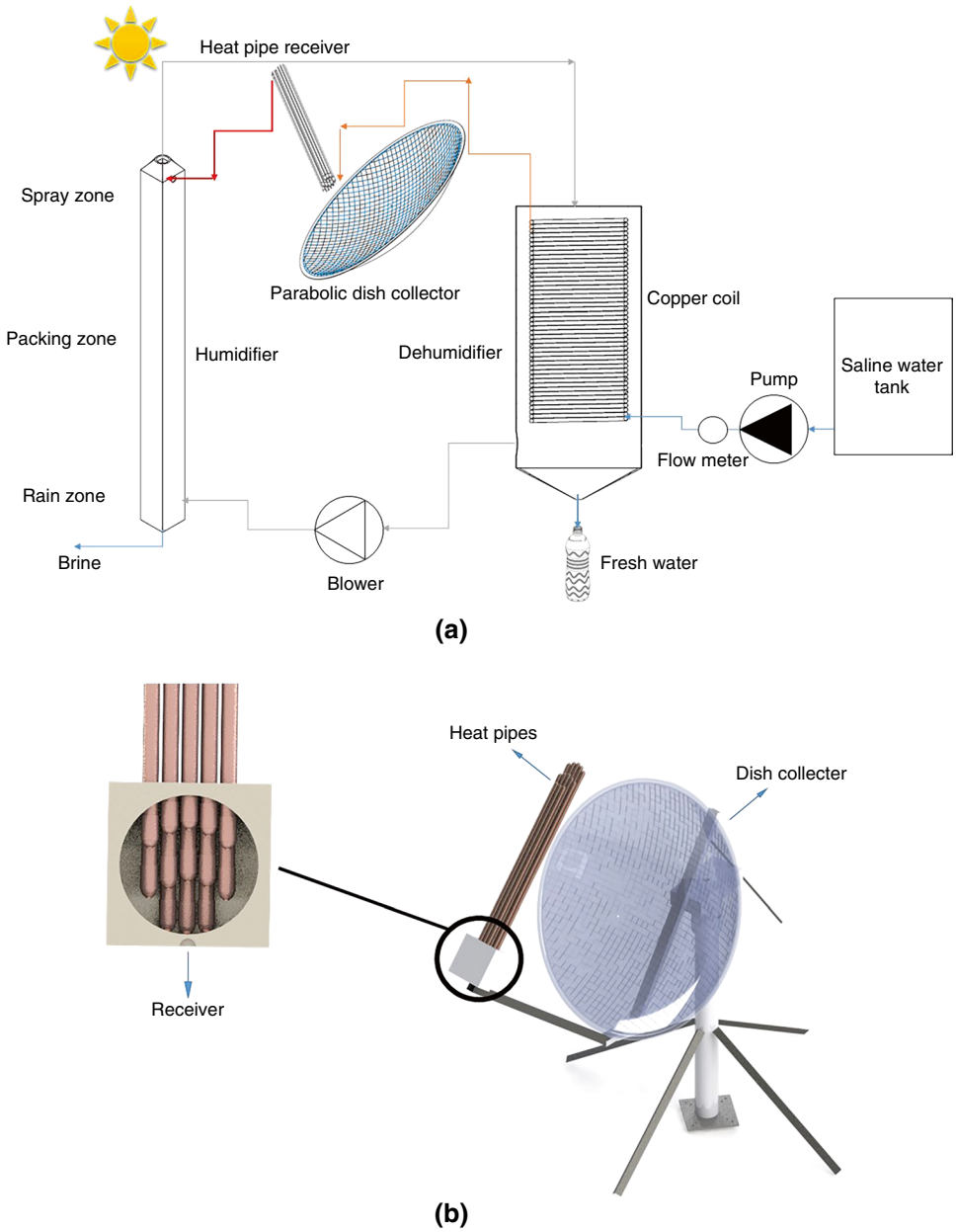

Fig. 2 **a** Schematic of the solar desalination system using the humidification–dehumidification method. **b** Heat pipes position with respect to the PDC

was reduced to 72 °C. Therefore, it can be concluded that incorporating extra evaporators into the heat pipe diminishes the evaporator's maximum thermal flux capacity located farthest from the condenser. Kumaresan et al. [37] have experimentally investigated the impact of different wick structures, including mesh, porous, and composite wick (porous mesh), in improving the efficiency of heat pipes, and have studied the impact of tilt angle and inlet heat. CuO nanofluid was used as the working fluid, which improved the heat transfer capacity by 12% compared to water. The maximum heat transfer capacity in the composite heat pipe was enhanced by 36%. Also, their results proved that the heat pipe's thermal resistance gradually decreases with the inclination angle increase. The highest drop for composite wick heat pipes at 45 angle was 47.50%, respectively. As mentioned above, heat pipes consist of a pipe inside with a wick and vapor flow. In the research of Ma et al. [38], steam methane reforming was investigated with a heat pipe consisting of two concentric pipes. A wick and sodium vapor flow were located in the larger pipe, and the smaller pipe was used as a reforming reactor. One of the noticeable results of their research was the creation of a uniform temperature on the entire wall of the reactor tube.

According to the literature, PDCs, as a heat source of the HDH desalination cycle, are effective in fully solarizing these desalination systems. Moreover, applying cavity receivers to PDCs was the most common approach studied in the literature. Regarding our best knowledge, according

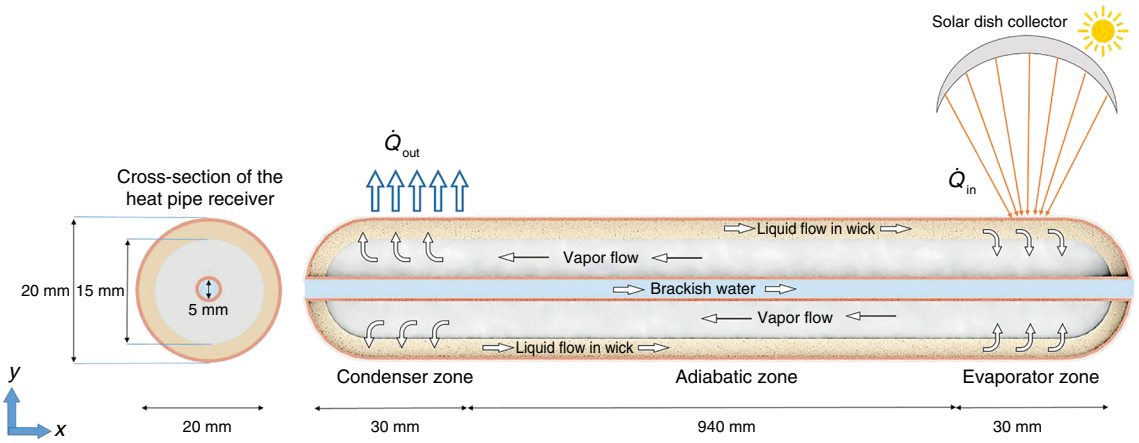

Fig. 3 The operation of the investigated heat pipe in the current study

Table 1 The structural parameters of the parabolic dish collector and the heat pipe

Structural characteristics of the heat pipe		Structural parameters of the parabolic dish collector [26]	
Heat pipe length	1000 mm	Diameter	1.8 m
Evaporator length	30 mm	Area	2.54 m^2
Condenser length	30 mm	Focal distance	1 m
Adiabatic zone length	940 mm	Reflectivity	0.84
Heat pipe outer diameter	20 mm	Concentration ratio	112
Heat pipe inner diameter	18 mm	Focal spot diameter	0.17 m
Brackish water hole outer diameter	7 mm		
Brackish water hole inner diameter	5 mm		
Wick thickness	2 mm		

to the literature, the heat pipe application has been rarely studied in the HDH desalination systems, and the novel application of heat pipe as a receiver of a PDC for brackish water heating can be an effective technique to enhance the desalination system performance. Hence, in the current study, a PDC-based HDH desalination cycle integrated with 13 heat pipes as the receiver of the parabolic dish was investigated numerically. The investigated parameters were the outlet brackish water temperature from the heat pipe in different solar flux conditions and the temperature and flow rates. Finally, a comparison has been made between the performance of the cavity receivers and heat pipes as the receiver of the PDCs in HDH desalination cycles.

Description of the proposed desalination system

The desalination system investigated in this study was based on the humidification–dehumidification method, which included a humidification column, a dehumidification column, and a solar heat source. According to Fig. 2 (a), the saline water is pumped through the copper coil inside the dehumidifier, acts as a cooling water, and then is directed to the solar collector. The heat source in this research was a parabolic dish collector with a heat pipe receiver (located in the focal spot of the dish (Fig. 2 (b)). The brackish water flows through the heat pipes and is heated to the HDH desalination system required temperature, which is 60 °C, and then directed to the humidifier to be sprayed into the humidification column. The sprayed hot water humidifies the counter-flow air upcoming air. Then, the humidified hot air flows to the condenser to reject its moisture content on the dehumidifier copper coil.

The current research project's heat pipe structure comprised two concentric copper tubes. The outer tube acts as a heat pipe, and the brackish water flows into the inner tube to gain heat. According to Fig. 3, the heat pipes' evaporator zone was located in the focal spot of the dish. Moreover, the condenser zone location with respect to the dish was variable based on the solar radiation angles to avoid shading on the dish reflector. The heat pipe and its wick's material were selected as copper, and the wick was a porous medium with a porosity of 0.5. The structural

characteristics of the investigated parabolic dish collector and the heat pipe are tabulated in Table 1. Moreover, there are three water samples (sample A, B and D with 3880, 10,600, and 21,500 ms cm^{-1} salinity) were described in terms of their salinity value (electrical conductivity) based on the Esfanjani et al. [25] research.

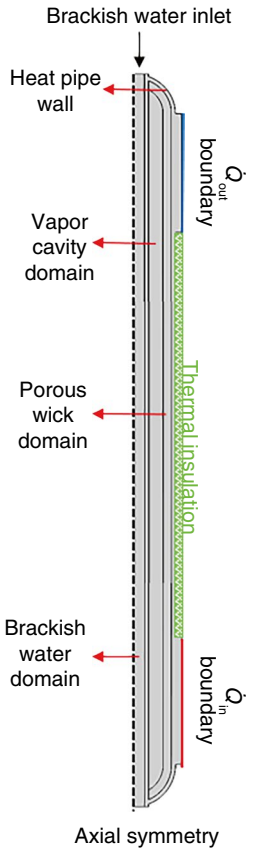

Fig. 4 The 2-D axial symmetry view of heat pipe schematic

The heat pipes in the proposed desalination system were designed so that the evaporator zone gains heat from the focused radiation of the dish. This process leads to the evaporation of the working fluid (distilled water). The generated vapor flows through the vapor cavity of the heat pipe to the condenser. Along with this, it rejects its heat to the brackish water hole inner wall and condensates to the liquid form. Then, the liquid flows through the wick and is directed to the evaporator zone. Apart from the conventional heat pipes, the condenser zone in this study cools down with the flowing brackish water inside the condenser and does not require other cooling water or fins, and the ambient air is sufficient for the cooling process of the condenser.

Governing Equations

The main equations utilized in this study for the simulation of the heat pipe were Navier–Stokes equations, including conservation of mass, momentum, and energy in the steady-state condition. The above-mentioned equations were solved with a COMSOL Multiphysics software. Conservation of mass was considered as the following equation [39].

$$\nabla \cdot \left(\rho \vec{V}\right) = 0 \tag{1}$$

The equation used for vapor flow thorough the vapor cavity was the momentum conservation equation in cylindrical coordinates (r, θ, z) as Eq. 2 [39].

$$\rho \frac{D\vec{V}}{Dt} = \nabla \cdot \left[-P \cdot I + \mu(\nabla \vec{V} + \left(\nabla \vec{V}\right)^T\right] \tag{2}$$

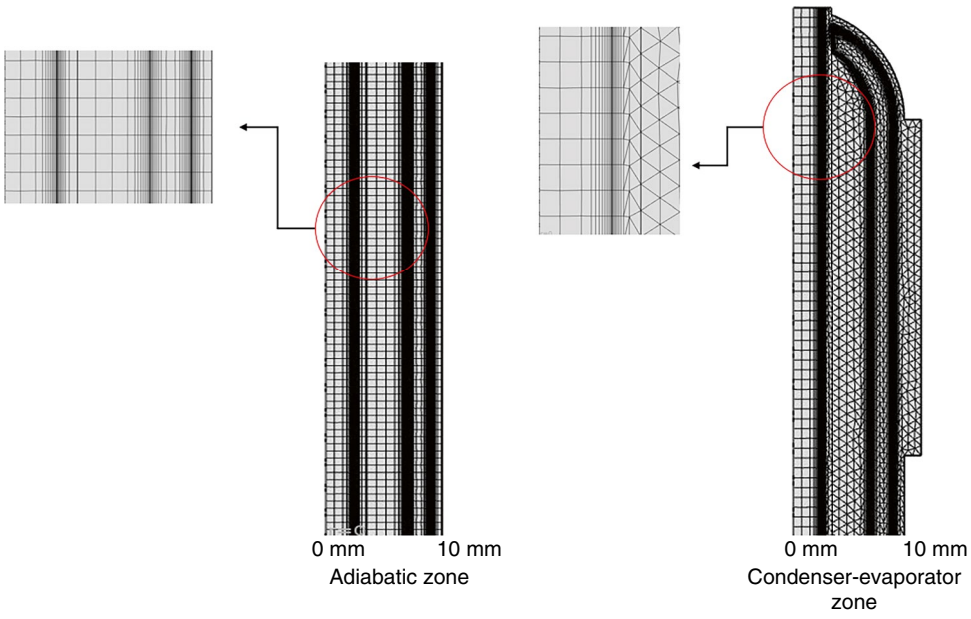

Fig. 5 The generated mesh for the current study

Table 2 Grid independency study in the current research

Number of elements	Outlet temperature of the brackish water/°C
4018	59.416
11,702	60.965
53,916	63.161
71,462	63.197
132,412	63.193

Also, energy conservation was obtained based on Eq. 3 [39]:

$$\rho C_{\mathrm{p}} \frac{DT}{Dt} = \nabla \cdot (k \nabla T) + Q \tag{3}$$

The first term is the derivative with respect to time-frame. The second is the spatial derivative of temperature. This term represents the divergence of the heat flux, describing how heat is distributed in space due to thermal conductivity k. and the third term accounts for the internal volumetric heat production. This energy equation was applied to the vapor, liquid, and solid copper tubes. Brinkman's equation for fluid flow in the porous wick was also utilized as follows.

$$\nabla \cdot [-P \cdot I + z] - \left(\mu K^{-1} + \beta \rho \left| \vec{U} \right| + \frac{Q_{\mathrm{m}}}{\varepsilon_{\mathrm{p}}^2} \right) \vec{U} = 0 \tag{4}$$

$$z = \mu \left(\nabla \vec{U} + \left(\nabla \vec{U} \right)^{\mathrm{T}} \right) - \frac{2}{3} \mu \left(\nabla \cdot \vec{U} \right) \rho \tag{5}$$

where Q_m is a mass source, which in this case was considered zero, and K is the permeability of the porous wick. According to the uniform temperature distribution of the brackish water hole inner wall, the mass flow rate of the outlet water from the heat pipe was determined as equation 6 to reach the sufficient desalination system's operating temperature.

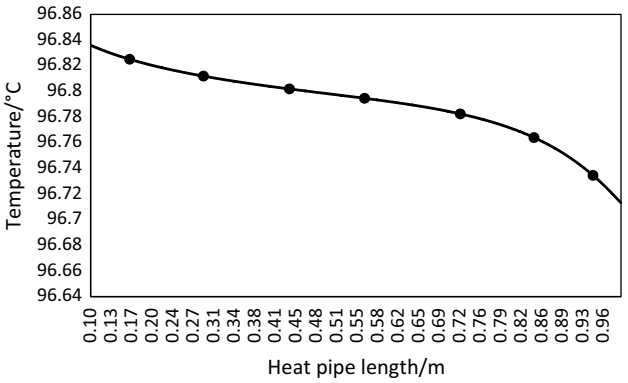

Fig. 7 Brackish water hole inner wall temperature distribution without water flow

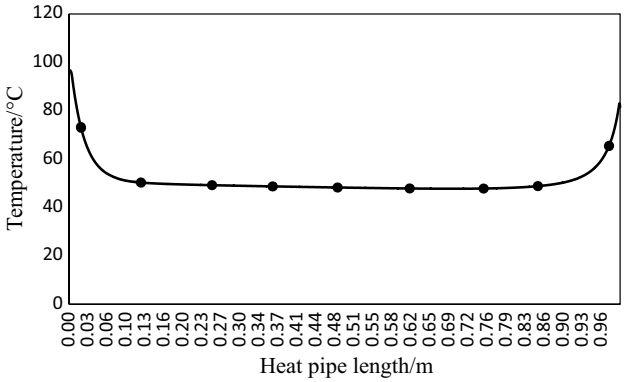

Fig. 8 Brackish water hole inner wall surface temperature distribution with water flow (water sample A, 0.3 L min^{-1})

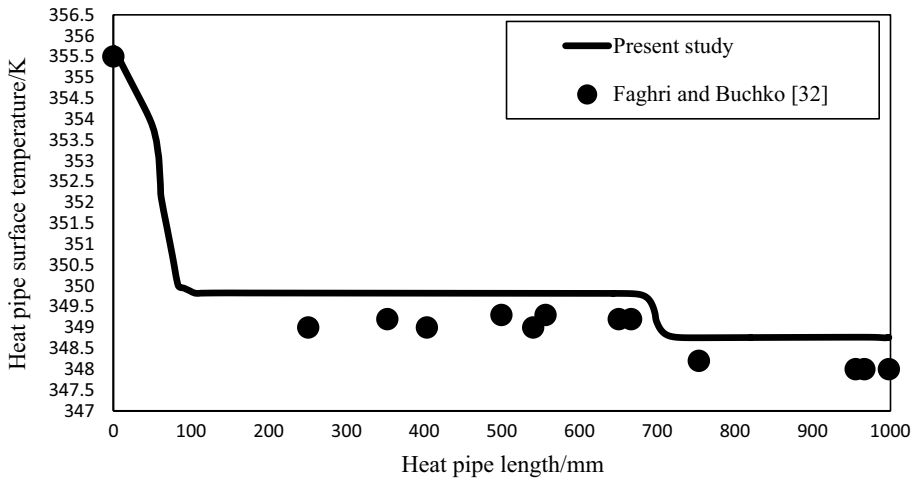

Fig. 6 Validation with Faghri and Buchko [36]

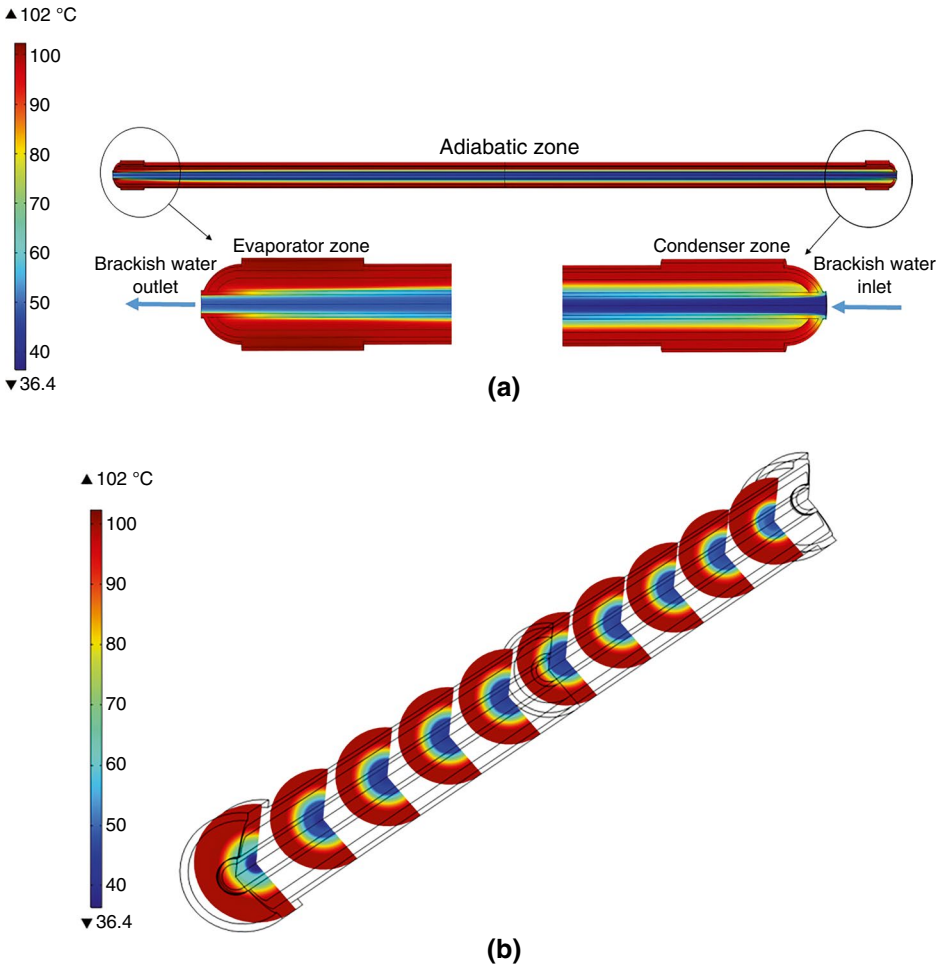

Fig. 9 Heat pipe temperature contour **a** longitudinal cross section **b** slice cross section at solar heat flux of 1007 W m^{-2}, (water sample A)

$$\dot{m} = \frac{Lph}{c_p \ln\left[\frac{T_s - T_{in}}{T_s - T_{out}}\right]} \tag{6}$$

Moreover, the thermal performance of the PDC with the utilization of heat pipe as a receiver in the current research was determined based on the following equation.

$$\eta_{th} = \dot{m} C_p \left(T_{out} - T_{in}\right) / G A_{dish} \tag{7}$$

where $T_{out} - T_{in}$ is the inlet and outlet's temperature difference of the brackish water of the heat pipe receiver.

Boundary conditions and assumptions

In this research, the heat pipe of the desalination system has been simulated and numerically solved in steady-state conditions. The solution method was selected as a laminar flow model (Reynolds numbers are 837, 43, 241 for vapor cavity, porous wick, and brackish water flow, respectively). The outlet brackish water flow was assumed fully developed. Moreover, Brinkman's equation for fluid motion and heat transfer in the porous medium was used. A fully coupled nonlinear solver was selected in the software. It should be mentioned that the finite element solver integrated all the investigated physics and solved the equations. The Newton–Raphson method was used based on the iterations to the initial guess until the solution converged. Convergence was obtained when the relative error between 2 successive iterations was of the defined order of tolerance. Also, the convergence value for mass and momentum conservation equations and energy conservation equations were considered 10^{-4} and 10^{-6}, respectively. For the numerical solution, the three-dimensional solution was omitted because of symmetrical geometry, and the problem was solved using axial symmetry boundary conditions. Due to the impact of the concentrated solar flux on half of the surface of the heat pipe, it was assumed that with the high copper metal's thermal conductivity, the flux would distribute over the entire evaporator surface. Contact resistance of the evaporator surface has also been neglected. Also, it was assumed that the wick was homogenous isotropic and permeability was selected 1×10^{-9} m^2. Moreover, the numerical data were

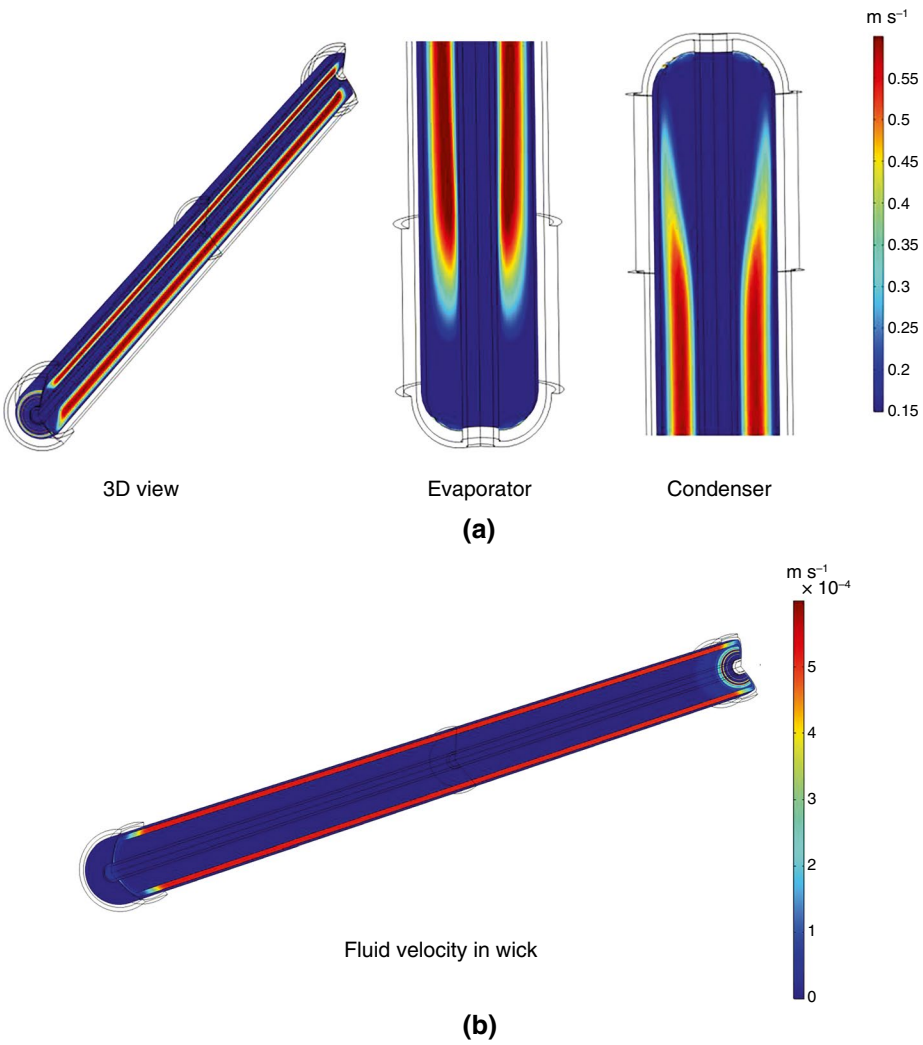

Fig. 10 Velocity contour of working fluid: **a** In vapor cavity, **b** In wick

compared with the experiments obtained from the research of Esfanjani et al. [25]. Furthermore, the desired flow rate for each heat pipe was selected 0.0375 L min^{-1}. Since there are 13 heat pipes in the focal spot of the collector, and the total flow rate of the outlet water of brackish water will be 0.4875 L min^{-1}. The 2-D axial symmetry view of the heat pipe schematic with boundary conditions details is illustrated in Fig. 4.

Grid and mesh independence study

The generated mesh for this study is depicted in Fig. 5. A grid study was done in the current research, and 71,462 elements were used for the simulations. The details of the grid study are tabulated in Table 2.

Results and discussion

First of all, it is worth mentioning that in order to validate the numerical solution of the current research, a heat pipe was simulated in the software according to the research of Faghri and Buchko [36], and the obtained results were compared with the research above according to Figure 6. As can be seen, there is a good agreement between the experimental reported by Faghri and Buchko [36] from the literature.

The temperature distribution of the brackish water hole inner wall without flowing water is depicted in Figure 7. As seen in this figure, the temperature distribution is uniform along the tube, and the maximum temperature difference was 0.25 from the inlet to the outlet of the heat pipe. Furthermore, the maximum and minimum temperature values of the inner wall of the heat pipe hole were 96.81 to 97.06 °C. Moreover, the temperature distribution of the brackish water hole inner wall surface with flowing water is

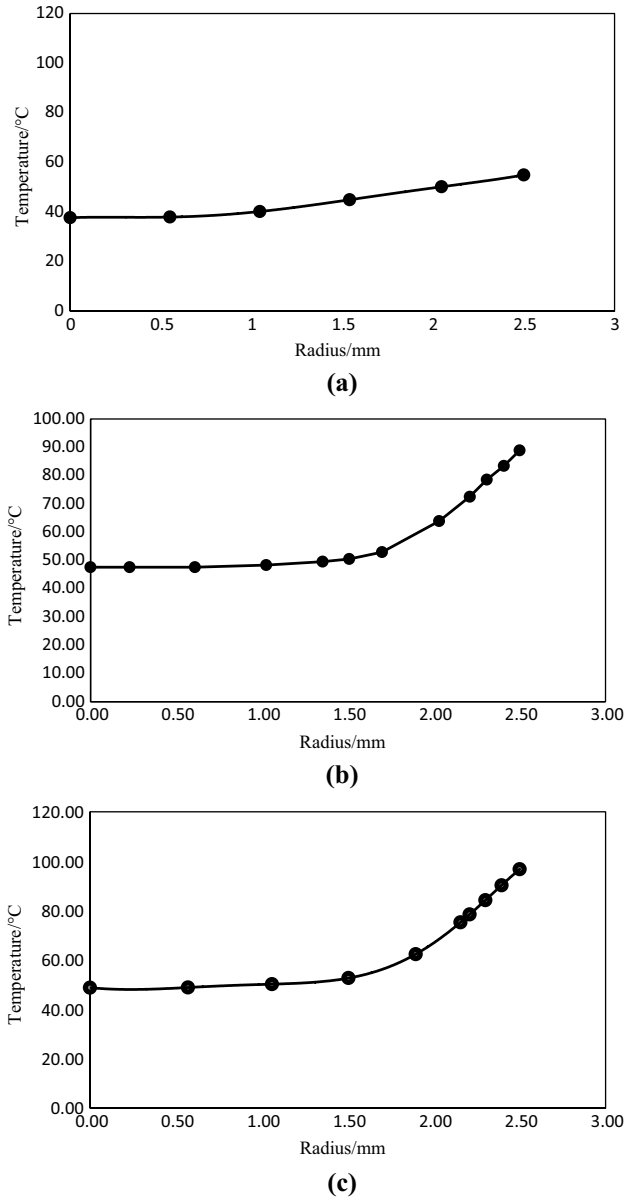

Fig. 11 Outlet cross-sectional brackish water tube temperature distribution: **a** brackish water temperature in condenser zone, **b** brackish water temperature in evaporator zone, **c** brackish water outlet temperature

illustrated in Figure 8. By flowing the brackish water in the hole, the maximum temperature difference of the brackish water hole inner wall for the evaporator and condenser was 15.25 °C and for the adiabatic zone was 2 °C.

Figure 9 depicts the temperature distribution of one heat pipe's cross section (longitudinal and slice view). The operating condition for this contour was solar heat flux of 1007 W m^{-2}, ambient temperature of 39.2 °C, and flow rate of 0.0375 L min^{-1}. As can be seen in this figure, the evaporator's vapor cavity temperature was 100 °C on

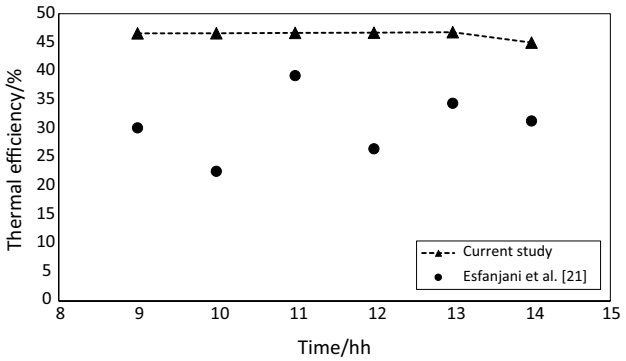

Fig. 12 comparison of the brackish water hole outlet temperature of current research with Esfanjani et al. experiments [25] (water sample A, 0.3 L min^{-1}n)

average. Hence, complete evaporation occurs, and the vapor temperature gradually decreases in the liquid phase. Moreover, Fig. 10 illustrates the working fluid velocity counter along the heat pipe. Inlet and outlet sections of the working fluid from the wick to the vapor cavity and from the vapor cavity to the wick are shown in this figure.

Figure 11 depicts the radial variations of the outlet cross section of the brackish water for case A in evaporator zone, condenser zone and outlet brackish water sections. The average outlet temperature was 63.98 °C. Also, the minimum temperature occurred in the center of the tube at 48.80 °C. Moreover, the maximum temperature was in radius of 2.42 mm from the center at 92.7 °C.

The outlet temperature of the brackish water hole between the current study and research by Esfanjani et al. [25] is illustrated in Figure 12. The data was compared hourly during the day for water sample A in flow rate of 0.3 L min^{-1}. As seen from the results, the heat pipe ensures a uniform water temperature throughout the day and, on average, leads to a higher temperature with respect to the cavity receiver (69.55 °C compared to 68.90 °C). In other words, the cavity receiver has more fluctuations in temperature but a higher maximum daily temperature (82.7 °C compared to 71.7 °C). It should be mentioned that despite the comparisons based on the flow rate of 0.3 L min^{-1}, this research focused on the flow rate of 0.4875 L min^{-1}, the maximum flow rate to meet the suitable temperature of the desalination system (60 °C) based on the experimental reference work. Hence, the produced freshwater flow rate increases with the brackish water flow rate increase. Moreover, the heat pipe's outlet temperature is tabulated in Table 3 for three water samples. The average outlet water temperature for cases A, B, and D in the flow rate of 0.4875 L min^{-1} were 61.94, 61.07, and 61.45 °C, respectively. Moreover, the maximum temperature for the water samples A, B, and D were 63.98, 61.51, and 64.37 °C, respectively.

Table 3 Heat pipe outlet brackish water temperature per time (0.4875 L min^{-1})

Time of the day	Solar radiation (Wm^{-2}) (Samples A, B, and C, respectively)	Sample A outlet temperature/°C	Sample B outlet temperature/°C	Sample D outlet temperature/°C
9	837–888	56.91	–	54.70
10	910–929	62.25	–	60.20
11	940,952,960	62.37	60.14	61.80
12	952,956,962	62.91	61.12	62.88
13	1,007,965,963	63.20	61.49	62.43
14	10,039,501,108	63.98	61.50	64.24

Table 4 Parabolic dish collector's thermal performance variations per time in current study (0.4875 L min^{-1})

Time of the day	Sample A thermal efficiency/%	Sample B thermal efficiency/%	Sample D thermal efficiency/%
9	35.65	–	35.56
10	35.66	–	35.57
11	35.69	33.93	35.56
12	35.72	35.73	35.73
13	35.75	35.76	35.76
14	34.54	35.79	32.30

Table 5 Maximum, minimum, and average thermal efficiency for three water samples in the current study (0.4875 L min^{-1})

Thermal efficiency/%	Sample A thermal efficiency/%	Sample B thermal efficiency/%	Sample D thermal efficiency/%
Maximum	35.75	35.79	35.76
Average	35.50	35.30	35.08
Minimum	34.54	33.93	32.30

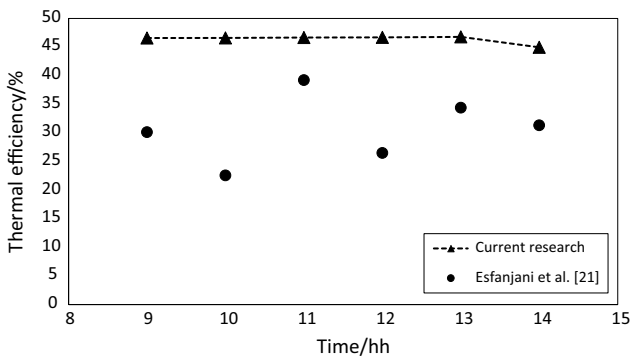

Fig. 13 Thermal efficiency comparison between current research and Esfanjani et al. [25] for water sample A (0.4875 L $min.^{-1}$)

The thermal performance values of the PDC with the utilization of a heat pipe as a receiver for the current desalination system for all the investigated water samples are tabulated in Table 4. As can be seen in Table 4, the thermal efficiencies are mostly uniform, with little changes in all the cases. Moreover, the highest, average, and lowest thermal performance values are presented in Table 4. Table 5 shows the highest maximum thermal performance for water sample B, with 35.79%. Furthermore, the highest average value for thermal efficiency belongs to water sample A, which is 35.50%, which is why water sample A is selected in most charts and tables.

Figure 13 compares the thermal efficiency values between current research and Esfanjani et al. [25] research for water sample A with a flow rate of 0.3 L min^{-1}. As presented in this figure, the heat pipe receiver has uniform thermal efficiency with an average of 46.38%. However, the cavity receiver of the Esfanjani et al. [25] research fluctuates more in terms of thermal efficiency values. Moreover, the average thermal efficiency difference between the heat pipe and cavity receiver was 15.69%.

Conclusions

The current research involves a numerical analysis of a cylindrical heat pipe in the application of an HDH desalination system. Saline water passes through the inner pipe, and by the focused solar radiation from the PDC on the heat pipe's evaporator zone, the required heat for the desalination is supplied. Some concluding remarks of this study are presented as follows.

- The heat pipe receiver ensures higher flow rate values, leading to higher freshwater production than the conventional cavity receivers.
- The highest thermal performance of the parabolic dish collector system, 35.79%, was determined for water sample B with a heat pipe receiver.
- The average thermal performance values of the parabolic dish collector system for cases A, B, and D were 35.50, 35.30, and 35.08%, respectively.

- The maximum outlet temperature for the cases A, B, and D were 63.98, 61.51, and 64.37 °C, respectively.
- The average outlet water temperature for cases A, B, and D in the flow rate of 0.4875 L min^{-1} were 61.94, 61.07, and 61.45 °C, respectively, and the temperature distribution along the inner pipe is uniform in all cases.

Author contributions Mohammad Afarideh, Pouya Esfanjani and Mohammad Sadegh Valipour contributed to conceptualization and methodology; Mohammad Afarideh involved in Numerical Simulation; Mohammad Afarideh and Pouya Esfanjani were involved in writing—original draft preparation and resources; and Mohammad Sadegh Valipour contributed to review, editing and supervision.

Funding The authors have no relevant financial or non-financial interests to disclose.

Declarations

Conflict of interest The authors declare that they have no known competing interest for this research work.

References

1. Shalaby S, Hammad FA, Zayed ME. Current progress in integrated solar desalination systems: Prospects from coupling configurations to energy conversion and desalination processes. Process Saf Environ Prot. 2023;178:494–510.
2. Lawal DU, Qasem NA. Humidification-dehumidification desalination systems driven by thermal-based renewable and low-grade energy sources: A critical review. Renew Sustain Energy Rev. 2020;125: 109817.
3. Karami M, Nasiri Gahraz SS. Transient simulation and life cycle cost analysis of a solar polygeneration system using photovoltaic-thermal collectors and hybrid desalination unit. Journal of Heat and Mass Transfer Research. 2021;8(2):243–56.
4. Sayed ET, Olabi A, Elsaid K, Al Radi M, Alqadi R, Abdelkareem MA. Recent progress in renewable energy based-desalination in the Middle East and North Africa MENA region. J Adv Res. 2023;48:125–56.
5. Dadashi Z, Mahmoudi A, Rashidi S. Capacity and strategies of energy production from renewable sources in Arab countries until 2030: a review from renewable energy potentials to environmental issues. Environ Sci Pollut Res. 2022;29(32):47837–66.
6. Bahoosh R, Nazeri A, Changizian M, Moravej M. Fabrication of Solar Desalination System and Experimental Investigation of its Performance of it, Located in Ahvaz City. Journal of Heat and Mass Transfer Research. 2022;9(2):255–68.
7. Mokhtar R. Y., Shouman M. A., Elmarghany M. R., and Hamed A. M., "Rethinking HDH desalination: A comprehensive review beyond energy towards, exergoeconomic. and renewable-based multigeneration evaluation," *Desalination.* 2024; 117286.
8. Belessiotis V., Kalogirou S., and Delyannis E., *Thermal solar desalination: methods and systems*. Elsevier, 2016.
9. Esfanjani P, Jahangiri S, Heidarian A, Valipour MS, Rashidi S. A review on solar-powered cooling systems coupled with parabolic dish collector and linear Fresnel reflector. Environ Sci Pollut Res. 2022;29(28):42616–46.
10. Akbarzadeh S, Valipour MS. Experimental study on the heat transfer enhancement in helically corrugated tubes under the non-uniform heat flux. J Therm Anal Calorim. 2020;140:1611–23.
11. Tayebi R, Akbarzadeh S, Valipour MS. Numerical investigation of efficiency enhancement in a direct absorption parabolic trough collector occupied by a porous medium and saturated by a nanofluid. Environ Prog Sustain Energy. 2019;38(2):727–40.
12. Faegh M, Behnam P, Shafii MB. A review on recent advances in humidification-dehumidification (HDH) desalination systems integrated with refrigeration, power and desalination technologies. Energy Convers Manage. 2019;196:1002–36.
13. Shaikh JS, Ismail S. Theoretical investigation on humidification–dehumidification desalination employing flat-plate solar water collector. J Therm Anal Calorim. 2023;148(21):11835–53.
14. Kalogirou SA. Solar thermal collectors and applications. Prog Energy Combust Sci. 2004;30(3):231–95.
15. Aboelmaaref MM, et al. Hybrid solar desalination systems driven by parabolic trough and parabolic dish CSP technologies: Technology categorization, thermodynamic performance and economical assessment. Energy Convers Manage. 2020;220: 113103.
16. Saddouri I, Rejeb O, Semmar D, Jemni A. A comparative analysis of parabolic trough collector (PTC) using a hybrid nanofluid. J Therm Anal Calorim. 2023;148(18):9701–21.
17. Jahangiri S, Alhamzawi A, Esfanjani P, Valipour MS, Akbarzadeh S. Impact of double-axis tracking on thermal performance of the linear Fresnel Collector: An experimental study. Sol Energy. 2024;272: 112483.
18. Akbarzadeh S, Valipour MS. Energy and exergy analysis of a parabolic trough collector using helically corrugated absorber tube. Renewable Energy. 2020;155:735–47.
19. Nazir MS, et al. A comprehensive review of parabolic trough solar collectors equipped with turbulators and numerical evaluation of hydrothermal performance of a novel model. Sustainable Energy Technol Assess. 2021;45: 101103.
20. Varol Y, Oztop HF. Buoyancy induced heat transfer and fluid flow inside a tilted wavy solar collector. Build Environ. 2007;42(5):2062–71.
21. Rahman M, Öztop HF, Ahsan A, Kalam M, Varol Y. Double-diffusive natural convection in a triangular solar collector. Int Commun Heat Mass Transfer. 2012;39(2):264–9.
22. Tiwari A, Kumar A. A comprehensive review on solar thermal desalination systems based on humidification-dehumidification approach. Clean Technol Environ Policy. 2023;25(7):2075–97.
23. Rafiei A, Loni R, Mahadzir SB, Najafi G, Pavlovic S, Bellos E. Solar desalination system with a focal point concentrator using different nanofluids. Appl Therm Eng. 2020;174: 115058.
24. Rafiei A, Alsagri AS, Mahadzir S, Loni R, Najafi G, Kasaeian A. Thermal analysis of a hybrid solar desalination system using various shapes of cavity receiver: Cubical, cylindrical, and hemispherical. Energy Convers Manage. 2019;198: 111861.
25. Esfanjani P, Mahmoudi A, Rashidi S, Valipour MS. Experimental investigation of a novel design of cavity receiver for a parabolic dish collector humidification-dehumidification desalination system. Energy Convers Manage. 2024;299: 117845.
26. Esfanjani P, Mahmoudi A, Valipour MS, Rashidi S. An experimental study on a cylindrical-conical cavity receiver for the parabolic dish collector. Environ Sci Pollut Res. 2023;30(3):6517–29.
27. Hemmatian A, Kargarsharifabad H, Esfahlani AA, Rahbar N, Shoeibi S. Improving solar still performance with heat pipe/pulsating heat pipe evacuated tube solar collectors and PCM: An experimental and environmental analysis. Sol Energy. 2024;269: 112371.

28. Jose J. and Hotta T. K.,"A comprehensive review of heat pipe: Its types, incorporation techniques, methods of analysis and applications," *Thermal Science and Engineering Progress,* p. 101860, 2023.
29. Yang M, Quan Z, Zhao Y, Wang L, Liu Z, Tang S. Experimental and numerical study on thermal management of air-cooled proton exchange membrane fuel cell stack with micro heat pipe arrays. Energy Convers Manage. 2023;275: 116478.
30. Ekka JP, Dewangan D. A comprehensive review on recent developments, applications and future aspects of heat pipe-assisted solar collectors. J Therm Anal Calorim. 2023;148(20):11173–201.
31. Liao X, Jian Q, Zu S, Li D, Huang Z. Visualization study and analysis on the heat transfer performance of an ultra-thin flat-plate heat pipe. Int Commun Heat Mass Transfer. 2021;126: 105464.
32. Riehl R, Buschmann M. Impact of particles on thermal performance of closed-loop oscillating heat pipe. Appl Therm Eng. 2024;236: 121413.
33. Khalid SU, Babar H, Ali HM, Janjua MM, Ali MA. Heat pipes: progress in thermal performance enhancement for microelectronics. J Therm Anal Calorim. 2021;143:2227–43.
34. Tian Z, et al. Experimental evaluation on heat transfer limits of sodium heat pipe with screen mesh for nuclear reactor system. Appl Therm Eng. 2022;209: 118296.
35. Behi H, et al. PCM assisted heat pipe cooling system for the thermal management of an LTO cell for high-current profiles. Case Studies in Thermal Engineering. 2021;25: 100920.
36. Faghri A. and Buchko M., "Experimental and numerical analysis of low-temperature heat pipes with multiple heat sources," 1991.
37. Kumaresan G, Vijayakumar P, Ravikumar M, Kamatchi R, Selvakumar P. Experimental study on effect of wick structures on thermal performance enhancement of cylindrical heat pipes. J Therm Anal Calorim. 2019;136:389–400.
38. Ma J, et al. Deciphering high-efficiency solar-thermochemical energy conversion process of heat pipe reactor for steam methane reforming. Fuel. 2022;326: 124972.
39. Jiji L. M. and Jiji L. M., *Heat convection*. Springer, 2006.